Chemical Engineering Journal 429 (2022) 130766

Contents lists available at ScienceDirect

Chemical Engineering Journal

journal homepage: www.elsevier.com/locate/cej

A composition-based model for methane adsorption of overmature shales in Wufeng and Longmaxi Formation, Sichuan Basin

Wenbin Jiang [a,b], Gaohui Cao [a,*], Chao Luo [c,d], Mian Lin [a,b,*], Lili Ji [a,b], Ji Zhou [a,b]

[a] Institute of Mechanics, Chinese Academy of Sciences, Beijing 100190, China
[b] University of Chinese Academy of Sciences, Beijing 100190, China
[c] PetroChina Southwest Oil & Gasfield Company, Chengdu, Sichuan 610051, China
[d] Shale Gas Research Institute of PetroChina Southwest Oil & Gasfield Company, Chengdu, Sichuan 610051, China

ARTICLE INFO

Keywords:
Shale gas
Wufeng-Longmaxi
Methane adsorption
Langmuir pressure
Clay

ABSTRACT

The Wufeng-Longmaxi Formation shale in Sichuan Basin is the main strata of shale gas exploration and development in China. Adsorbed methane is an important part of the total shale gas content. The influence of shale composition on adsorption characteristics is complex, and it is difficult to obtain a comprehensive understanding without a sufficient amount of data. In this work, the total organic carbon (TOC), X-ray diffraction (XRD) mineral analysis, and the excess methane adsorption isotherms with pressure up to 50 MPa at 40 °C of 106 overmature shale samples with TOC of 0.8%-9.0% and clay content of 2%-58% that belong to Wufeng-Longmaxi formation from 10 shale gas wells in Sichuan Basin, China are experimentally investigated and analyzed. New correlations found between compositions and methane adsorption characteristic parameters guide the establishment of a composition-based methane adsorption model that the excess adsorption isotherm of shale is the content-weighted sum of equivalent unit-content excess isotherms for organic matter and clay. With this model, the differences of excess isotherms of these two compositions and the differences of clay-contribution to methane adsorption for different sublayers are disclosed. It is beneficial to improve the accuracy of shale reservoir evaluation of studied blocks under the condition of limited coring and deepening the understanding of the underlying mechanism of methane adsorption characteristics.

1. Introduction

The black shales from the Upper Ordovician Wufeng Group (O_3w) and the lower part of Lower Silurian Longmaxi Group (S1l) in the Sichuan Basin are currently the main strata for shale gas exploration and development in China [1,2]. The shales of these layers have relatively high organic matter content, developed nano-pores, large specific surface area, and have strong adsorption capacities for methane which is the main component (more than 95%) of shale gas [3–5]. Adsorption increases the total gas content of shale reservoirs, which is higher than that of conventional natural gas reservoirs under the same formation temperature, pressure, porosity, and gas saturation. On the other hand, the adsorbed gas amount changes with pressure, resulting in a different dynamic process of gas production from conventional natural gas [6–10]. Therefore, it is very important to accurately obtain the variations of adsorbed methane amount of gas-bearing shales.

The isothermal adsorption experiment is the main method to obtain the adsorbed methane amount of shale samples [11]. In the early stage, studies were mainly conducted on shale with relatively shallow burial depth and low formation pressure. The maximum balance pressure of the isothermal adsorption experiment was generally lower than 20 MPa. The results showed that the amount of adsorbed methane increased first, then there is a slight decrease or increase or flattening as pressure increases [12–24]. In recent years, researchers have used gravimetric and volumetric methods to conduct isothermal adsorption experiments in higher pressure ranges. More and more studies have shown that the measured adsorption isotherms have the characteristic of first rising and then falling as pressure increases [25–34]. Researchers have modified the classical adsorption models to fit experimental excess adsorption isotherms through the addition of adsorbed-phase density [35,36]. The results show that the modified Langmuir model and Toth model both can fit the measured excess adsorption isotherms well [37]. Of the two, the modified Langmuir model only has three parameters, namely the Langmuir volume V_L, the Langmuir pressure P_L, and the adsorbed-phase

* Corresponding authors at: Institute of Mechanics, Chinese Academy of Sciences, Beijing 100190, China.
E-mail addresses: caogaohui@imech.ac.cn (G. Cao), linmian@imech.ac.cn (M. Lin).

https://doi.org/10.1016/j.cej.2021.130766
Received 17 March 2021; Received in revised form 3 June 2021; Accepted 5 June 2021
Available online 10 June 2021

density ρ_{ads}, which are the simpler.

Establishing relationships between adsorption characteristic parameters and geochemical, mineralogical, and petrophysical parameters is a key issue geologically for scientists and engineering. Several studies have been carried out on the Wufeng-Longmaxi shale in the Sichuan Basin. Existing studies mainly focus on the maximum adsorption capacity (represented by V_L) and have clarified that it positively correlates with TOC (total organic content) and specific surface area. Some studies have shown that the clay also has a certain contribution to methane adsorption [12,15,18,38–41]. The mechanism that V_L relates to adsorption sites that can be provided by organic matter and clay minerals together is easier to understanding. Unlike V_L, there are few discussions about P_L and ρ_{ads} [35,42–44] that relate to the change of adsorption amount with pressure. The understanding of the controlling factors of the differences in the shapes of excess isotherms is still very limited. Researches are often conducted on a small number of samples in a well or multiple wells. The correlations have not been comprehensively examined and analyzed, and whether existing ones are applicable in a wider range is uncertain [26,27,43,45]. In this study, 106 shale samples from the Upper Ordovician Wufeng Group (O_3w) and the lower part of Lower Silurian Longmaxi Group (S1l) in 10 shale gas wells in the Sichuan Basin, China are experimentally investigated. The total organic content (TOC), mineral composition, and high-pressure adsorption isotherms at the same temperature and pressure range of these samples were measured. The distribution of these parameters and their correlations are comprehensively analyzed. A composition-based model for methane adsorption amount under different pressures proposed based on the correlations result and the existing understanding of shale gas adsorption mechanism. The article is arranged as follows: Section 2 introduces the sample information and the methods used in this work, Section 3 introduces the results and discussion, and finally, conclusions are drawn.

2. Samples and methods

2.1. Samples' information and schematic workflow

The 106 studied shale samples with burial depth between 1500 m and 4400 m are from the Wufeng Formation (O_3w) and the $S_1l_{11}^1$- $S_1l_{11}^4$ sublayers of Longmaxi Formation (S_1l) of 10 wells in the Sichuan Basin, China. The locations of the wells are depicted in the upper-left corner of Fig. 1, including the AS31, BS22, NS2, RS7, RS2, RS4, RS5, TS2, BS13,

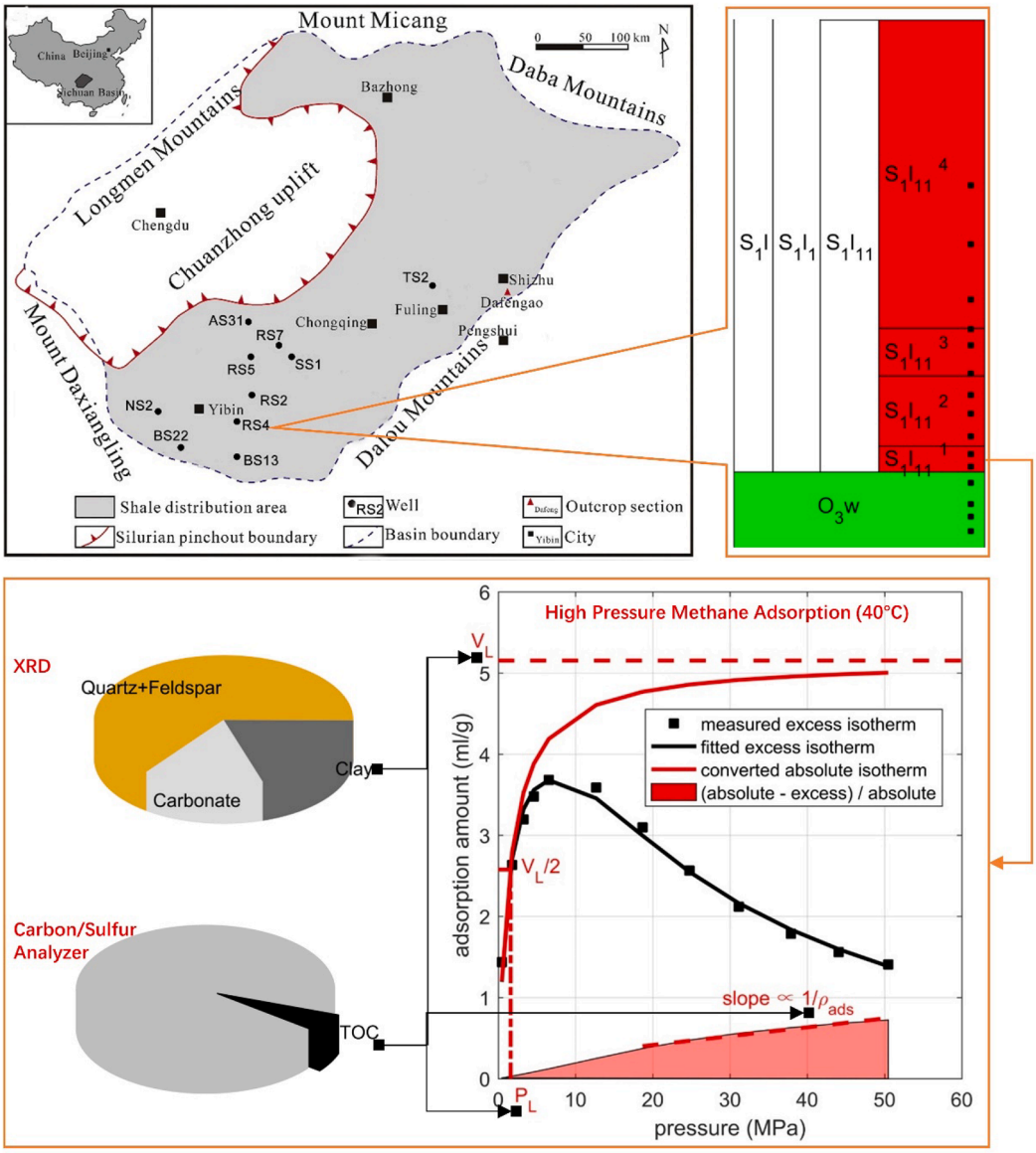

Fig. 1. The locations of studied shale gas wells and the schematic workflow of this study.

and SS1 wells that belong to the Changning, Weiyuan, Luzhou, and Yuxi blocks of PetroChina. For each well, 6–18 samples are selected, and the upper-right corner of Fig. 1 shows the distribution of samples in the vertical direction in the RS4 well, for example. The TOC, XRD mineral content (lower-left corner of Fig. 1), and high-pressure methane adsorption isotherm (lower-right corner of Fig. 1) are measured for each sample. V_L, P_L, and ρ_{ads} are the typical characteristic parameters for methane excess adsorption isotherms (details about their control on the isotherm shape in Section 2.3). Correlations between TOC, mineral content, and thses parameters are performed to instruct the construction of the composition-based model.

2.2. Experimental approaches

2.2.1. TOC, mineral content analysis

The samples are analyzed at Keyuan Engineering Testing Center, Sichuan, China. Before analysis, all shale samples were pretreated to meet the requirements of the experiment. TOC was measured using a Leco CS-400 carbon/sulfur analyzer. Firstly, hydrochloric acid was used to remove inorganic carbon in samples. After drying, the de-carbonated samples were heated to 1200 °C under oxygen flow to convert the organic carbon into carbon dioxide. Mineral compositions were determined using an X-ray diffractometer (XRD). All the samples were crushed into a fine powder and then analyzed with a Panalytical X'Pert PRO MPD X-ray diffractometer with Cu Kα radiation (40 kV, 40 mA) at a scan rate of 2°/min over an angular range of 5°–45°.

2.2.2. Methane isothermal adsorption experiment

About 100 g of the crushed and sieved sample with a diameter between 0.84 mm and 2.36 mm (8 to 20 Mesh) are used to measure methane adsorption isotherm. This mesh size is chosen considering the proximity to the core and the ease of sample preparation. Before analysis, the samples are all dried and vacuumed at 110 °C for 7 h to fully exhaust the impurity gas and water content in the inner void space.

The measurement is all performed at 40 °C using a high-pressure gas adsorption analyzer (3H-2000PH690, developed jointly by the Institute of Mechanics, Chinese Academy of Sciences and BeiShiDe Instrument) with the operating temperature range of 20 °C-140 °C and the pressure range of 0–69 MPa using the volumetric method. It is known that the adsorption amount is influenced by temperature and pressure. To control variables, the temperature is set to be the same. The influence of the temperature on methane adsorption is not the focus of this work and will be investigated in the future. Considering that the adsorption amount decreases as temperature increases, measurements at relative-low temperature (40 °C) will have a higher signal-to-noise ratio. Additionally, it is safer, high efficient, and more energy-saving.

The excess adsorbed amount $V_{ex}(p_{i+1})$ (ml/g) at the (i + 1)th balance pressure point p_{i+1} (MPa) is determined following Eq. (2).

$$V_{ex}(p_{i+1}) = V_{ex}(p_i) + \frac{22400\left(\frac{p_i V_{sample}}{Z_i} + \frac{p_{i+1/2} V_{base}}{Z_{i+1/2}} - \frac{p_{i+1} V_{base} + p_{i+1} V_{sample}}{Z_{i+1}}\right)}{mRT} \quad (2)$$

where V_{base} is the volume of the base chamber (ml), V_{sample} is the void volume of the sample chamber (ml) including the void space of the sample when the sample is loaded, $p_{i+1/2}$ is the intermediate pressure (MPa) of the base chamber after the methane intake when the valve between the base chamber and the sample chamber is closed, Z_i, $Z_{i+1/2}$ and Z_{i+1} are the compressibility factors at the corresponding pressures, m is the mass of the sample, T is the temperature (K), and R is the universal constant of gas (8.31441 J/mol/K). The Setzmann and Wagner (Se-W) equation of state (EOS) which is proved to predict free methane density at high pressure more accurately than Peng-Robinson EOS [46,47], is used to determine the free-gas density and compressibility factor of methane at different pressure [48].

2.3. Fitting of adsorption isotherms

The modified Langmuir equation (MLE, Eq. (3)), which includes three parameters (V_L, P_L, and ρ_{ads}) is often used to fit an excess isotherm $V_{ex}(p)$

$$V_{ex}(p) = \left(\frac{V_L p}{p_L + p}\right)\left(1 - \frac{\rho_{free}}{\rho_{ads}}\right) \quad (3)$$

where V_L denotes the maximum adsorbed amount (g/ml), P_L denotes the Langmuir pressure (MPa), ρ_{ads} denotes the adsorbed-phase density (g/cm^3), and ρ_{free} denotes the free-gas density (g/cm^3) at pressure p (MPa). It should be noted that the mathematical form of the modified Langmuir equation is utilized here because it has fewer parameters that have relatively clear physical meaning that is easy to understand. It does not mean the methane adsorption in shales under the reservoir condition follows Langmuir monomolecular layer adsorption mechanism.

As shown in the lower-right corner of Fig. 1, P_L corresponds to the pressure where the adsorption amount reaches 1/2 of the maximum adsorption amount. It can be used to represent the rate of initial increase of the adsorption amount with pressure. The smaller the P_L, the faster the rising speed. ρ_{ads} correlates to the descending slope of the isotherm at the high-pressure range. The higher the ρ_{ads}, the smaller the absolute value of the descending slope. These three parameters have certain physical meanings, which can help to understand the characteristics of methane adsorption.

3. Results and discussion

3.1. TOC and mineral composition

The distributions of TOC and XRD clay content (TClay for short) are shown in Fig. 2. The TOC values of the studied samples range from 0.8% to 9.0%, with an average value of 3.5%. The TClay values range from 2% to 58%, with an average value of 24.5%, while the XRD quartz content ranges from 9% to 77%, with an average value of 42.5%.

Fig. 2 shows the histograms (bars) of TOC and TClay with the fitted mean (μ) and standard deviation (σ) listed above the graphs. Performing Jarque-Bera hypothesis tests [49] with null hypotheses that TOC and TClay follow the normal distribution, respectively. P-values are 0.5, 0.08, which are larger than 0.05, indicating that TOC, TClay are normally distributed. The fitted normal-distribution probability density functions (dotted line) are also depicted in Fig. 2. The normal-distribution characteristics of data provide a basis for subsequent correlation analysis and enhance the statistical significance of analysis.

From the mineralogical ternary diagram shown in Fig. 3, it can be seen that in general, the quartz and feldspar content of shale in these layers are relatively higher, with an average of 51.3%. The average clay content is 24.5%, and the average carbonate content is 23.9%. In terms of sublayers (Fig. A1), samples of $S_1l_{11}{}^1$ have the highest quartz content overall. Samples of $S_1l_{11}{}^2$ have a relatively higher carbonate content than samples of $S_1l_{11}{}^3$ and $S_1l_{11}{}^4$ overall. Samples of $S_1l_{11}{}^4$ have a relatively higher clay content than samples of $S_1l_{11}{}^3$, and samples of $S_1l_{11}{}^3$ have a higher clay content than samples of $S_1l_{11}{}^2$ overall. The mineral components of the studied samples cover a wide range, which can ensure that the relationships obtained here have a wide range of applicability.

3.2. Methane adsorption characteristic parameters

The adsorption isotherms at 40 °C for all samples are shown in Fig. 4. The adsorption isotherms of all samples show a trend of rising first and then falling as pressure increases. The reason is that what can only be obtained by experiments is the excess adsorbed amount, that is, the amount of gas in the adsorbed phase that exceeds the bulk phase. The total amount of gas in the adsorbed phase is generally called the absolute

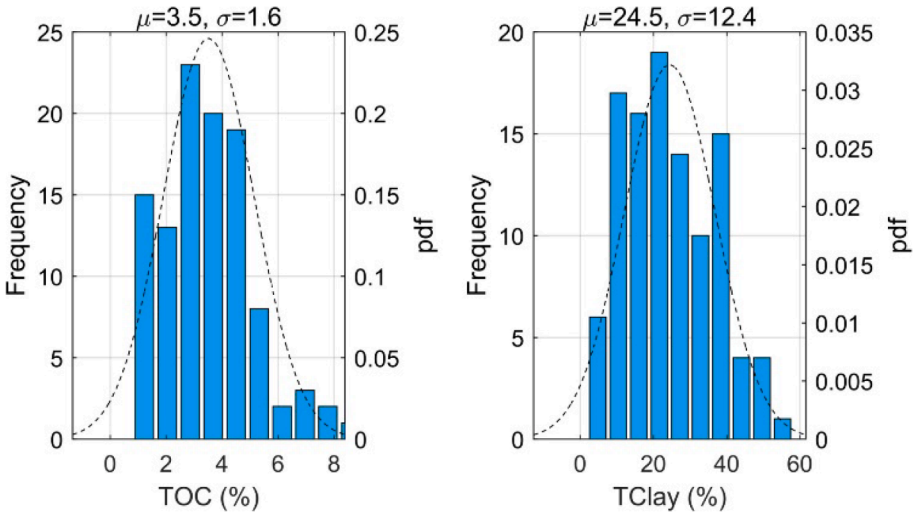

Fig. 2. Distributions of TOC and TClay.

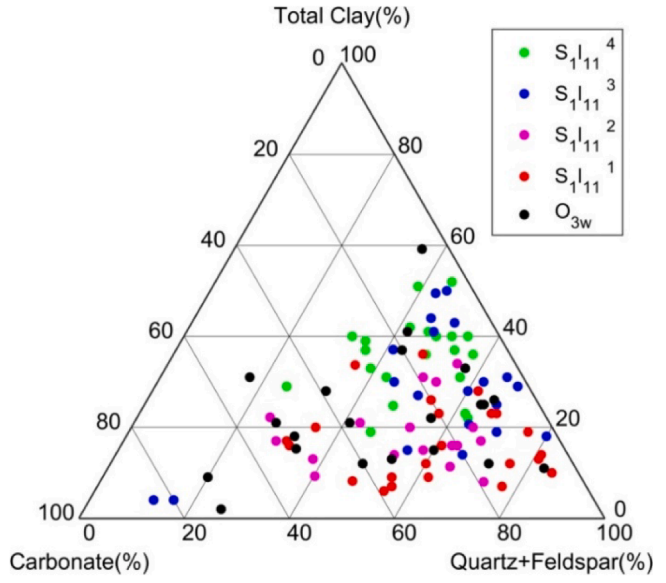

Fig. 3. Ternary diagram of the XRD mineral composition for the study shale samples.

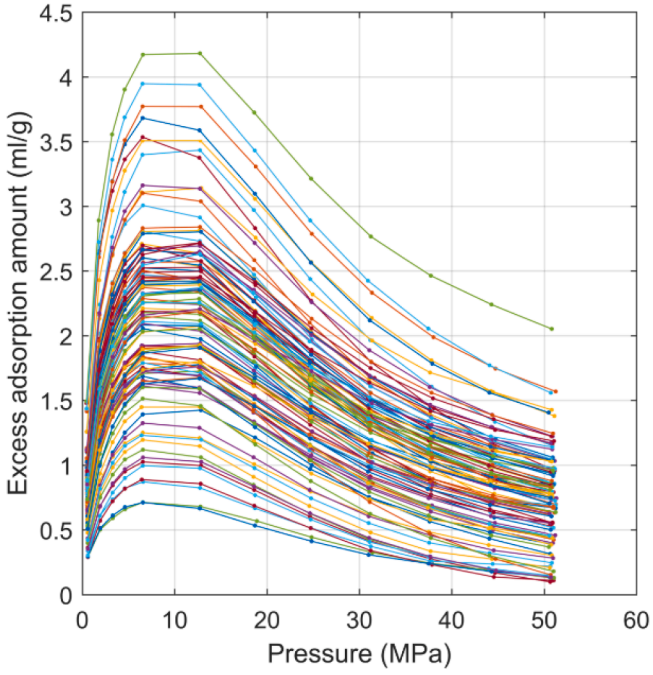

Fig. 4. Adsorption isotherms at 40 °C of the studied samples.

adsorbed amount. At low pressure, the bulk-phase density is significantly smaller than the adsorbed-phase density, and the difference between excess and the absolute adsorbed amount is small. At high pressure, the bulk-phase density is comparable with the adsorbed-phase density, and the difference between the excess and the absolute adsorption amount becomes greater. As the pressure increases, the adsorbed phase approaches saturation, and the growth rate of adsorbed-phase density is slower than that of bulk-phase density. Therefore, the excess adsorbed amount shows a downward trend as pressure increases. This mechanism is well demonstrated by the molecular simulation of methane adsorption in nanochannels [37].

The conversion from the excess adsorbed amount to absolute adsorbed amount has a variety of schemes and different results due to the different methods used to determine the adsorbed-phase density [37]. From the perspective of total gas content, without conversion, it can be determined directly based on excess adsorbed amount and porosity, gas saturation, temperature, and pressure [50]. Therefore, it is more direct and unique to use excess adsorption isotherm to describe the gas adsorption characteristic of shale samples.

The three-parameter Langmuir equation (Eq. (3)) was used to fit all the adsorption isotherms, respectively. All the fittings are satisfactory. The minimum value of adjust R^2s obtained was 0.98, the maximum value was 1.0, and the average value was 0.99. Therefore, the variation of adsorbed amount with pressure can be described with the three-parameter Langmuir equation, V_L, P_L, and ρ_{ads}. It is more convenient to use three parameters instead of isotherms with 10–12 data points for further analysis and predictions.

The V_L of all samples ranges from 1.1 ml/g to 5.9 ml/g, with an average of 3.3 ml/g. P_L ranges from 1.3 MPa to 3.6 MPa, with an average of 2.2 MPa. ρ_{ads} ranges from 0.27 g/cm^3 to 0.42 g/cm^3, with an average of 0.34 g/cm^3.

Fig. 5 shows the distribution of these three parameters. Performing Jarque-Bera hypothesis tests with null hypotheses that the above three parameters follow the normal distribution, respectively, p-values are 0.50, 0.09, and 0.50, which are larger than 0.05, indicating that the V_L, log(P_L), and ρ_{ads} values are normally distributed. The mean values and

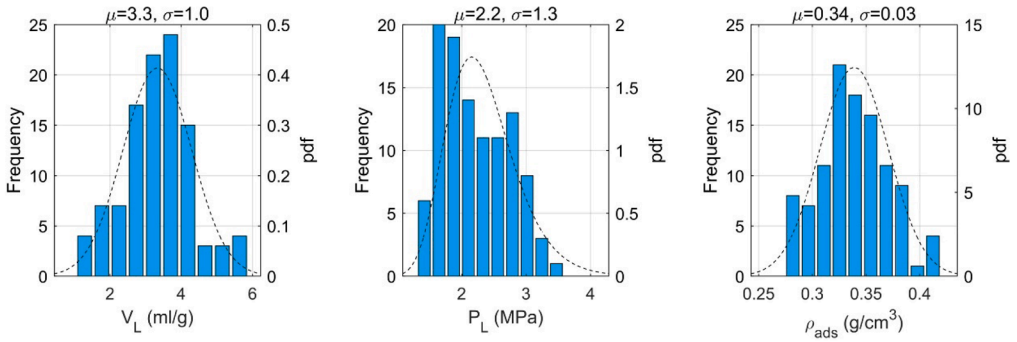

Fig. 5. Distributions of V_L, P_L, and ρ_{ads}.

the standard deviations of V_L, P_L, and ρ_{ads} are determined by distribution fitting and are listed above the figures in Fig. 5.

The maximal information coefficient (MIC) and Pearson correlation coefficient r [51] are used to analyze the correlations between V_L, P_L, and ρ_{ads}. The MIC can identify both potential linear and nonlinear relationships [52] and is calculated using the minepy library [53] in this work. For data with MIC larger than 0.5 and linear relationship indicated from the scatter plot, Pearson correlation coefficient is used to further evaluate the strength of correlation. Further, the data points are also linearly fitted, and the determined adjusted R^2 (adjusted r-square, an indicator for the goodness of fit) are calculated and used as another indicator of relevance. It can be seen from Fig. 6 that the points are somewhat scattered in a wide band. The MICs for correlations between the every two of V_L, P_L, and ρ_{ads} are all smaller than 0.5, indicating that V_L, P_L, and ρ_{ads} are relatively independent and need to be analyzed separately.

3.3. Correlations between geochemical, mineralogical, and methane adsorption parameters

Gasparik et al., (2012) observed that the overall sorptive potential and the shape of excess sorption isotherm of shales is a rather complex function of organic and inorganic composition and maturity (and hence, the pore structural character) of shales and suggested that investigations involving a multivariate statistical approach on a larger data set are necessary to elucidate the role of each of these variables in the gas sorption process in shales [14]. The studied shales in this work are overmature and the variations of TOC-normalized maximum adsorption capacity and P_L are small according to existing researches [42,54] at the overmature stage. Therefore, the correlations between the geochemical (TOC), mineralogical (XRD clay content) and methane adsorption (V_L, P_L, and ρ_{ads}) parameters are mainly analyzed to disclose the main controlling factors that affect the adsorption characteristics. V_L, P_L, and ρ_{ads} are analyzed, respectively.

3.3.1. V_l

Studies have indicated that the dominant adsorption process of methane on shales belong to physical adsorption [25] and are controlled by the physical (van der Waals forces) bonding of the gas and the solid molecules. Given that V_L represents the theoretical maximum absolute sorption capacity, it relates to the number of adsorption sites that might be provided by organic matters and minerals. Therefore, multivariate linear fitting with a zero intercept (Eq. (4)) can be done between V_L and TOC, TClay, quartz, and feldspar (XQF), carbonate content (XCA) to investigate the contributions to adsorption sites of different contents.

$$V_L = b_1 TOC + b_2 XCC + b_3 XQF + b_4 XCA \quad (4)$$

The best-fitting parameters and corresponding standardized regression coefficient (src) are listed in Table 1. The standardized regression coefficients [55] indicate the strength of the relation between V_L and each component. TOC and TClay are found to be the two main controlling factors of V_L, as their standardized regression coefficients are an order of magnitude larger than others. Based on this, organic matter and clay minerals probably provide most of the adsorption sites. Therefore, the correlations between methane adsorption characteristic parameters and TOC, TClay in the subsequent sections.

The correlations have been performed between the Langmuir volume V_L and TOC, TClay to further analyze the effect of TOC and clay content. It can be seen from Fig. 7 that V_L and TOC have a strong positive linear correlation with a MIC of 0.70 and a Pearson r of 0.78, and the adjusted R^2 of the linear fitting is 0.61. This relationship has also been reported for other shales [24,54,56,57]. Considering the direct correlation

Table 1
Best-fitting parameters for Eq.(4).

	1 (TOC)	2 (TClay)	3 (XQF)	4 (XCA)
b_i	0.546	0.043	0.006	0.003
src_i	0.917	0.554	0.089	0.058

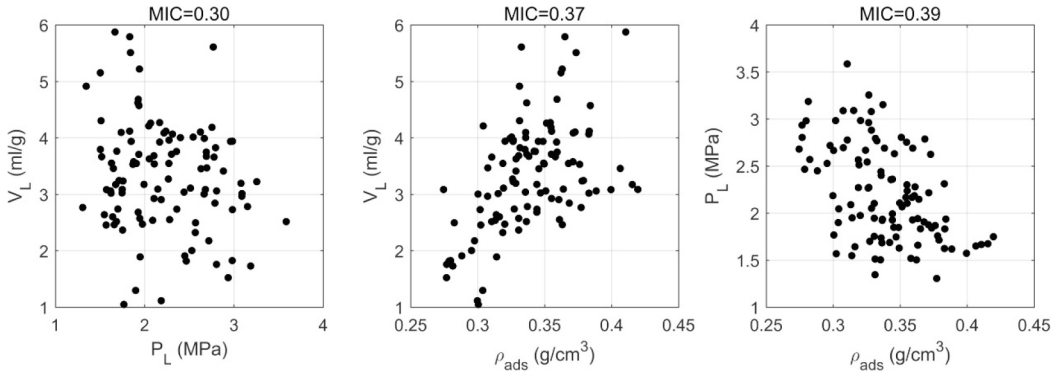

Fig. 6. Correlations of V_L, P_L, and ρ_{ads} of the studied shale samples.

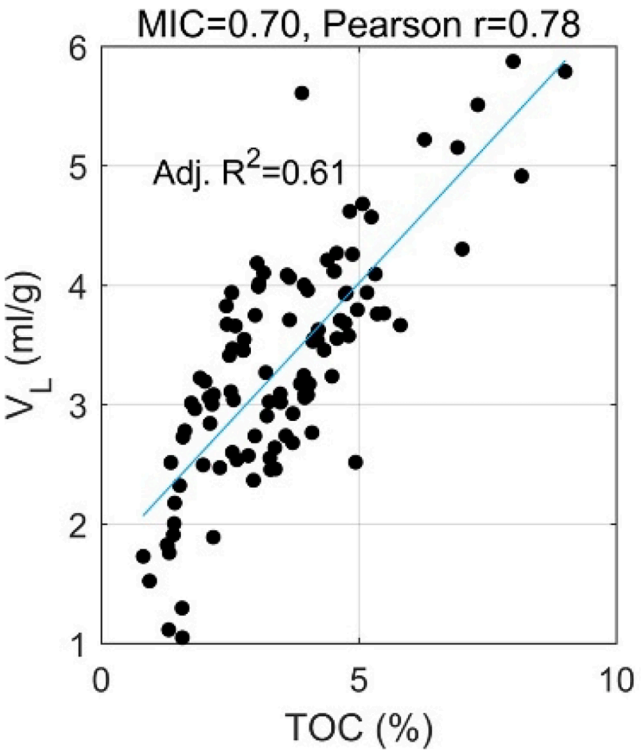

Fig. 7. Correlations between V_L and TOC.

analysis between V_L and TClay may be interfered with by TOC due to the variation of TOC with the same TClay for different samples, TOC-normalized V_L is used instead. Fig. 8 indicates that clay content also has a positive influence on V_L, which indicates that the adsorption sites can be provided by clay minerals. It can be supported by scanning electron microscopy images that clay interlamellar pores are the most common interparticle pores in Wufeng-Longmaxi shale and are believed as the most significant inorganic pores for hydrocarbon considering

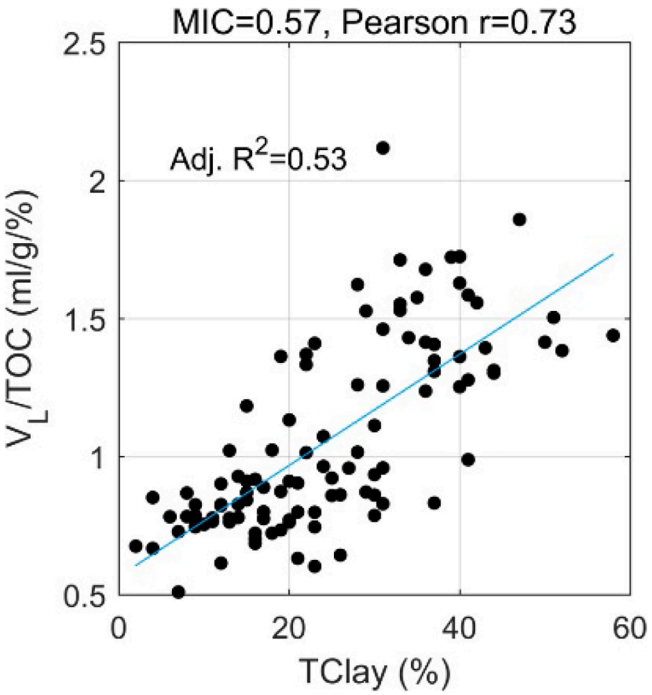

Fig. 8. Correlations between TOC-normalized V_L and TClay.

their quantity and connectivity [58].

3.3.2. P_l

Langmuir pressure P_L can represent the shape of the low-pressure section of an excess adsorption isotherm. Lower P_L indicates that methane is adsorbing more readily at lower pressure and the affinity of solid surface for methane is higher. The correlations between the Langmuir pressure P_L and TOC, TClay are shown in Fig. 9. It can be seen that there are negative and positive linear correlations between P_L and TOC, TClay, respectively. In other words, these two trends are exactly opposite, that is, P_L decreases with increasing TOC but increases with increasing clay content.

Just looking at the correlations between P_L and TOC, the explanation might be that affinity increases for high organic content [42]. However, it cannot explain the decrease of P_L with increasing TClay as the relationships between affinity and content should be in the same direction. From the perspective of the physical adsorption mechanism, the possible explanation might be that P_L of organic matter and clay basically do not change with their respective contents or change little, and the variations of P_L of shale are mainly caused by the different combinations of the two. It can be supported by the correlation between P_L and the ratio of TClay to TOC shown in Fig. 10 and the goodness of fit (adjusted $R^2 = 0.74$) is significantly higher than any of Fig. 9. It can be inferred that P_L of organic matter is smaller than the P_L of clay minerals indicating that the affinity of methane to organic matter is stronger than to clay minerals which is consistent with existing understandings [24,59].

3.3.3. ρ_{ads}

ρ_{ads} can represent the shape of the high-pressure section of an excess adsorption isotherm. The correlations between the adsorbed-phase density ρ_{ads} and TOC, TClay are shown in Fig. 11. It can be seen that the ρ_{ads} and TOC are somewhat positively linear correlated and the points are scattered in a wide band with MIC = 0.61 and Pearson r = 0.59. The MIC for ρ_{ads} TClay is 0.26, indicating weak correlations. Assuming that similar to P_L, ρ_{ads} of a single component basically unchanged or change little with the content, based on the above correlation analyses, it can be inferred that the value of ρ_{ads} of organic matter is larger than that of clay minerals.

3.4. A composition-based predictive models for shale methane adsorption amount

Through multivariate statistical analyses on the large data set of 106 shale samples from different layers and wells, it is possible to disclose the complex function between methane adsorption characteristics and composition. The excellent fit of the excess adsorption isotherms of the samples indicates that the modified Langmuir equation (MLE, Eq. (3)) with V_L, P_L, and ρ_{ads} can capture the maximum adsorption capacity along with the shape, namely, the variations of adsorption amount with pressure.

The fact that the main adsorption sites (indicated by V_L) are provided by organic matter and clay minerals is relatively clear as it can be supported in several ways [60], including the founded organic and clay pores from SEM images [58], the positive correlations between V_L and TOC, TClay and also the dual-site adsorption equation of shale gas proposed by Tang et al., [61]. In comparison, there is still a big gap in the understanding of how organic matter and clay control the shape of adsorption isotherms. Previous researchers have superimposed the adsorption isotherms of kerogen and pure clays and compared them with the isotherms of shale [13,15,19] and found it is only valid for some samples. It has been found that samples collected from outcrops or shallow wells might be unrepresentative for shale gas exploration [14]. Whether the pure clays or kerogen extracted from a specific sample can represent the inorganic and organic of real shales is still questionable.

Through the foregoing analysis, it is believed that the shape of excess isotherm at low pressure (indicated by P_L) is controlled by the

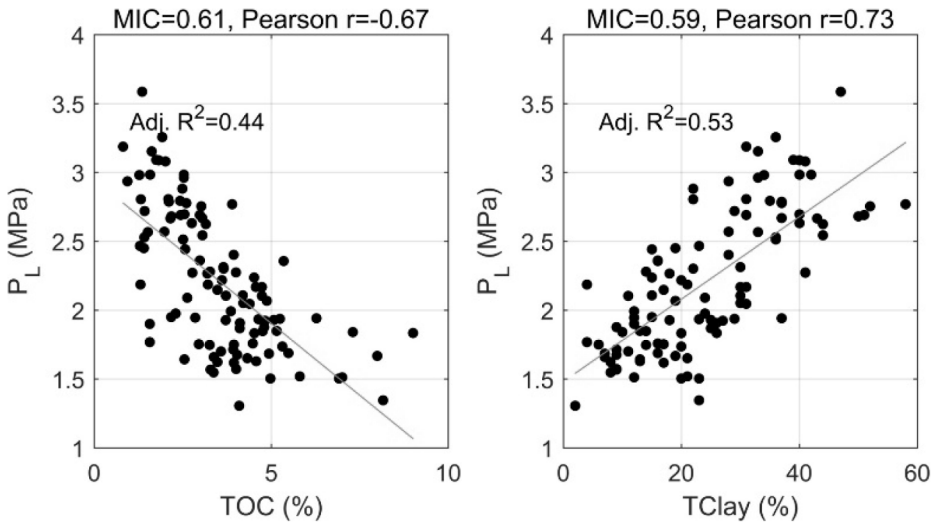

Fig. 9. Correlations between P_L and TOC, TClay.

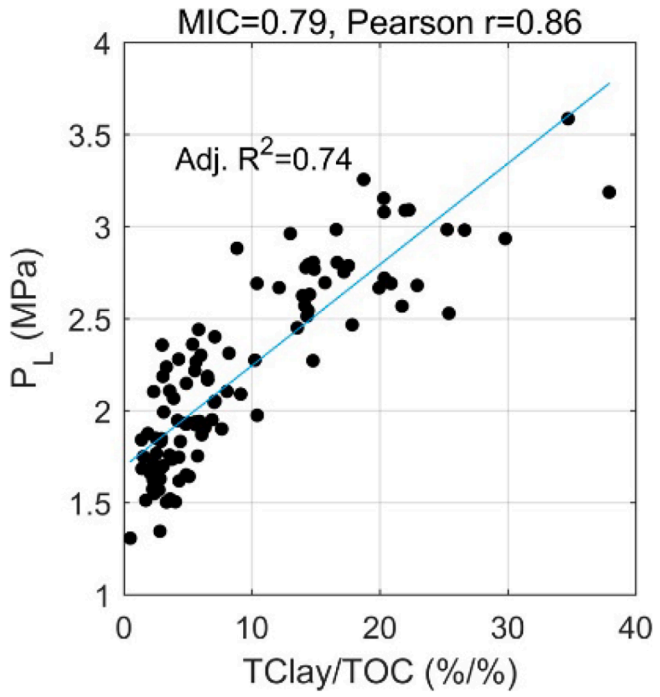

Fig. 10. Correlations of P_L with TClay /TOC.

composition of organic matter and clays rather than their individual contents. The shape at high pressure (indicated by ρ_{ads}) has a similar characteristic with high probability. Therefore, it is reasonable to put forward the hypothesis that for overmature shale in the studied area and formations the difference between isotherms of unit organic matter and clay is significantly greater than the possible difference within them that may be caused by the differences in maturity of organic matter, clay mineral type composition, pore size distribution, and other aspects, and an equivalent excess isotherm can be given for the organic matter and clay mineral respectively. A composition-based model can be proposed that the excess adsorption isotherm of shale is the content-weighted sum of equivalent unit-content excess isotherms for organic matter and clay as follows.

$$V_{ex}(p) = TOC\left(\frac{V_{L_{org}}p}{p_{L_{org}}+p}\right)\left(1-\frac{\rho_{free}}{\rho_{ads_{org}}}\right) + TClay\left(\frac{V_{L_{clay}}p}{p_{L_{clay}}+p}\right)\left(1-\frac{\rho_{free}}{\rho_{ads_{clay}}}\right) \quad (5)$$

where, $V_{L_{org}}$, $p_{L_{org}}$ and $\rho_{ads_{org}}$ are the three characteristic parameters of the methane adsorption isotherm for a unit (1% TOC) organic matter, and $V_{L_{clay}}$, $p_{L_{clay}}$ and $\rho_{ads_{clay}}$ are those for unit (1%) clay content. In this study, there are 10 to 12 data points (pressure p versus adsorbed amount V_{ex}) in a measured adsorption isotherm for each sample, and the number of data points in total is 1270 with 106 shale samples. These six unknown parameters can be determined through the nonlinear fitting of the 1270p-V_{ex} data. The initial values of $V_{L_{org}}$ and $V_{L_{clay}}$ for nonlinear fitting are b_1 and b_2 of Eq. (4); Those of $p_{L_{org}}$ and $p_{L_{clay}}$ are the smallest and largest values obtained from experiments, respectively, and those of $\rho_{ads_{org}}$ and $\rho_{ads_{clay}}$ are the largest and smallest experimental values, respectively.

The best-fitting results are listed in Table 2, and the adjusted R^2 is 0.92. Predictions using Eq. (5) and the best-fitting parameters are done on the 1270 data point and show a strong linear correlation with the experimental results with a Pearson r of 0.96, and the average and standard deviation of errors are 0.0 and 0.2 ml/g, respectively (Fig. 12). 95% of the errors are distributed between −0.40 ml/g and 0.48 ml/g, Therefore, the composition-based model is quite acceptable in engineering applications.

The predicted excess isotherms with the model for 0.6% TOC, 10% TClay and different combinations of TOC and TClay are plotted in Fig. 13 to provide an intuitive impression of the equivalent excess adsorption isotherms of the organic matter and clays . he maximum excess adsorption amount of 0.6% TOC is close to that of 10% TClay, while the organic matter adsorbs methane more readily than the clay mineral at low pressure and the methane adsorption amount decreases slowly at high pressure for organic matter.

The predicted excess isotherms with the model for 0.6% TOC, 10% TClay and different combinations of TOC and TClay are plotted in Fig. 13 to provide an intuitive impression of the equivalent excess adsorption isotherms of the organic matter and clays . The maximum excess adsorption amount of 0.6% TOC is close to that of 10% TClay, while the organic matter adsorbs methane more readily than the clay mineral at low pressure and the methane adsorption amount decreases slowly at high pressure for organic matter.

Fig. 14 shows the distribution of TClay/TOC of the studied samples. It can be seen that a certain number of samples has a ratio larger than 10, and the median value of TClay/TOC for the samples of the S_1l_{11}[4]

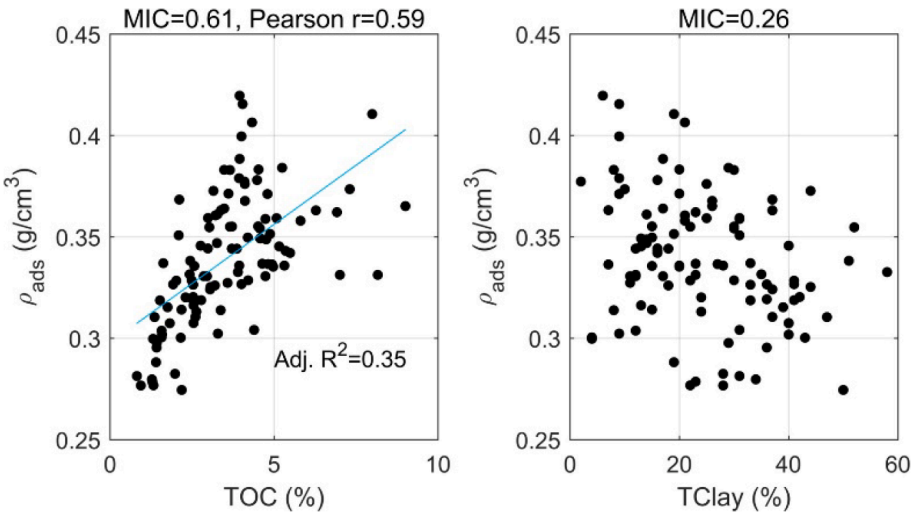

Fig. 11. Correlations between ρ_{ads} and TOC, TClay.

Table 2
Best-fitting parameters for Eq.(5).

Parameter	$V_{L_{org}}$ (ml/g)	$p_{L_{org}}$ (MPa)	$\rho_{ads_{org}}$ (g/cm^3)	$V_{L_{clay}}$ (ml/g)	$p_{L_{clay}}$ (MPa)	$\rho_{ads_{clay}}$ (g/cm^3)
Value	0.606	1.31	0.384	0.059	6.78	0.277

sublayer is over 15 and the contribution of clay to the total adsorption is comparable to that of organic matter. The contribution of clay is lowest in the $S_1l_{11}{}^1$ sublayer overall.

With the model, the excess adsorption isotherm with a wider range of combinations of TOC (0–10%) and TClay (0–80%) can be calculated and fitted with Eq. (3) to determined V_L, P_L, and ρ_{ads}. The variations of these three parameters with content are shown using contour (left) and 3D surfaces (right) in Figs. 15, 16, and 17, respectively. The black squares in the left graph and the three-dimensional scatter bars in the right both denote the experimental data and the fitted experimental parameters in this study. The magnitudes of the parameters are indicated by the colors of the surfaces and bars, also the heights of the bars. The changing trend with TOC and TClay and magnitude of fitted experimental adsorption parameters are generally consistent with those of the fitted predicted parameters. The fluctuation of ρ_{ads} is relatively larger among the three, which may be due to its small variation range, and that it correlates the descending slope of the isotherm at high-pressure range which may be influenced by other unknown factors that need further investigation, such as pressure sensitivity of sample skeleton volume, etc [60].

It can be seen that the relationship between V_L and TOC, TClay is approximately bilinear, and a weak nonlinear phenomenon exists when TOC is low and Clay is high. Therefore, it is easier to be identified by multivariate linear fitting. Due to the nonlinearity of the modified Langmuir equation, the changing of P_L and ρ_{ads} with TOC and TClay show great deviations from a bilinear relationship on the whole. It should be noted that the understanding obtained through correlation analysis is sensitive to samples that are used, and it might have considerable limitations without a sufficient number of samples with various compositions.

With this model, it is able to quickly and relatively accurately predict methane excess adsorption isotherms at 40 °C for the overmature Wufeng-Longmaxi shale in the Sichuan Basin, China once the geochemical and mineralogical parameters are obtained. Furthermore, the adsorbed amount at different temperatures can also be further predicted using existing relationships such as the adsorption potential theory, adsorption heat theory, etc. [20,44,45,62], which is beyond the scope of this study and will be investigated in future work.

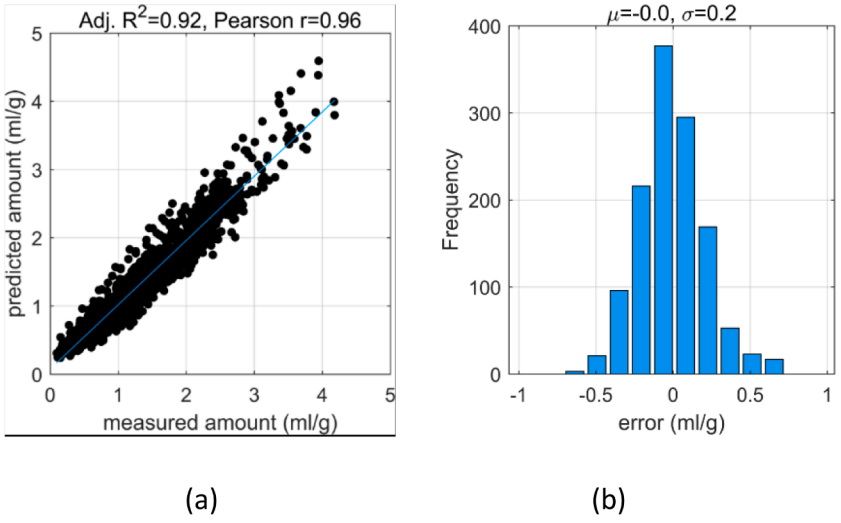

Fig. 12. Correlations between predicted and measured amount (a) and error distribution (b).

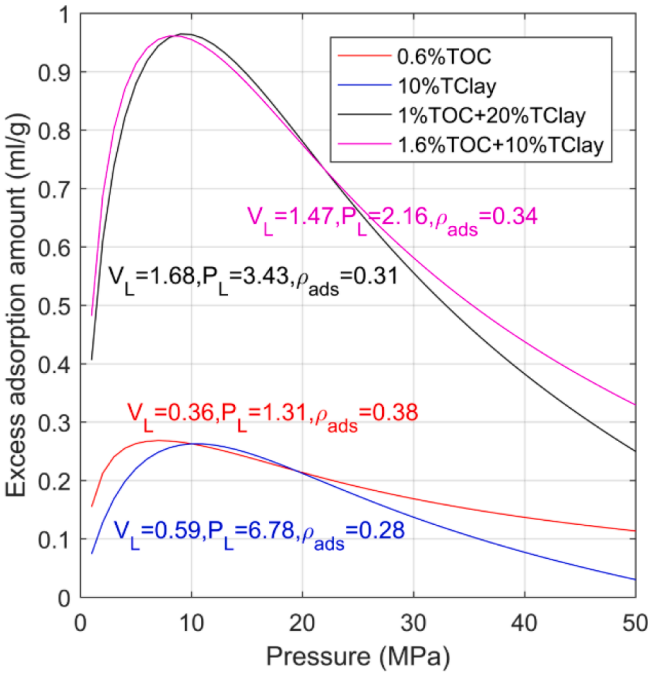

Fig. 13. Predicted excess isotherms for 0.6% TOC, 10% TClay and different combinations of TOC and TClay.

4. Conclusion

The study aims to disclose the complex relationship between organic, inorganic composition and adsorption capacity, shale of excess adsorption isotherm that continues to receive attention but has not been fully understood. Composition analyses and methane adsorption experiments with pressure up to 50 MPa are performed on 106 shale samples with TOC of 0.8%-9.0% and clay content of 2%-58% that belong to Wufeng-Longmaxi formation from 10 shale gas wells in Sichuan Basin, China. The studied parameters all follow normal distributions, except that P_L follows lognormal distribution, which ensures that the understanding obtained here has a wide range of adaptability. With such a large data set, correlations between compositions and adsorption characteristic parameters promote the understanding of the roles of compositions on shale gas adsorption which includes: i) the main compositions that control methane adsorption characteristics are organic matter and clay in the studied formations and blocks, ii) the shape of excess isotherms is controlled by the composition of organic matter and clays rather than their individual contents, iii) organic matter adsorbs methane more readily than clay at low pressure and has an isotherm with a slower drop in high-pressure section. A composition-based methane adsorption model has been proposed that the excess adsorption isotherm of shale is the content-weighted sum of equivalent unit-content excess isotherms for organic matter and clay. With this model, it is determined that shales from $S_1l_{11}^4$ sublayer have a larger clay-contribution to methane adsorption than those from $S_1l_{11}^1$ sublayer.

This model is proposed for the overmature shale samples in Wufeng and Longmaxi Formation, Sichuan Basin, China. The corresponding equivalent unit-content excess adsorption isotherms for each

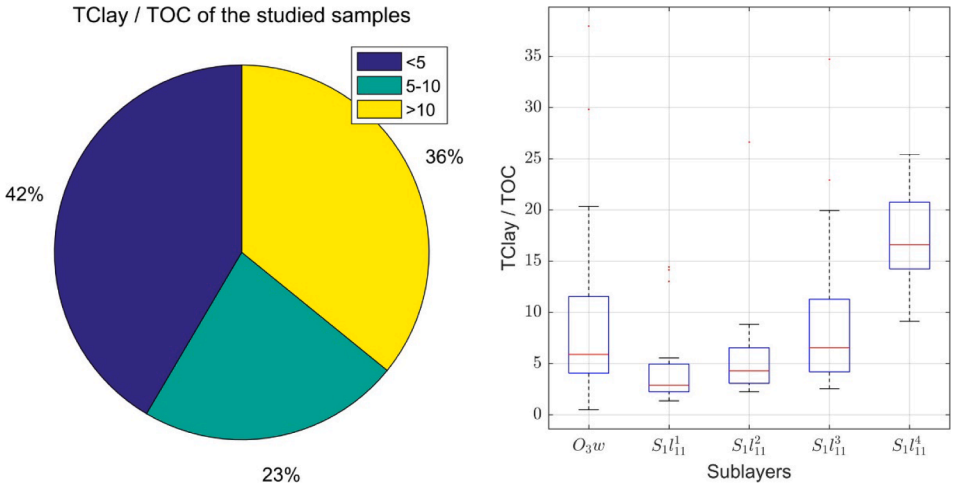

Fig. 14. The pie plot (a) and boxplot (b) of TClay/TOC of the studied samples.

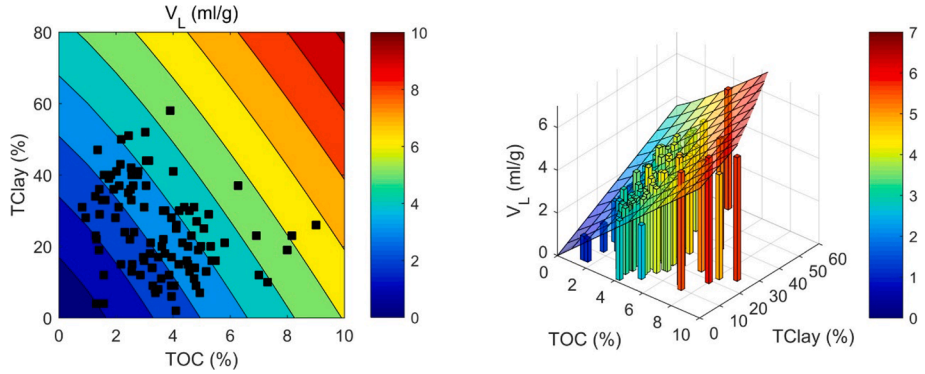

Fig. 15. Variation of V_L with TOC and TClay.

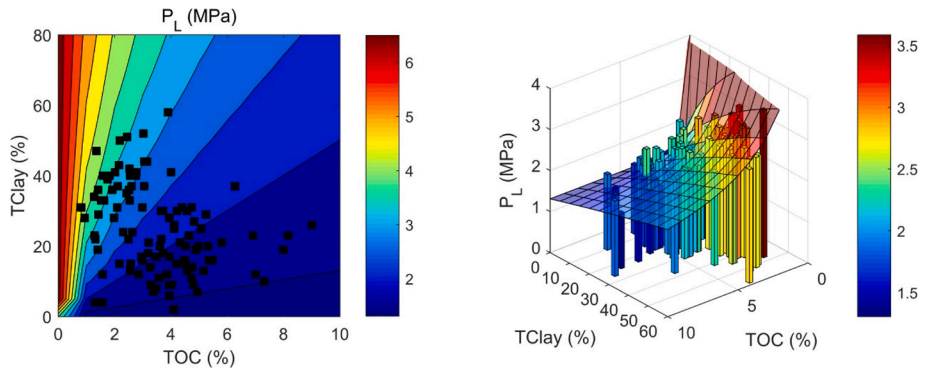

Fig. 16. Variation of P_L with TOC and TClay.

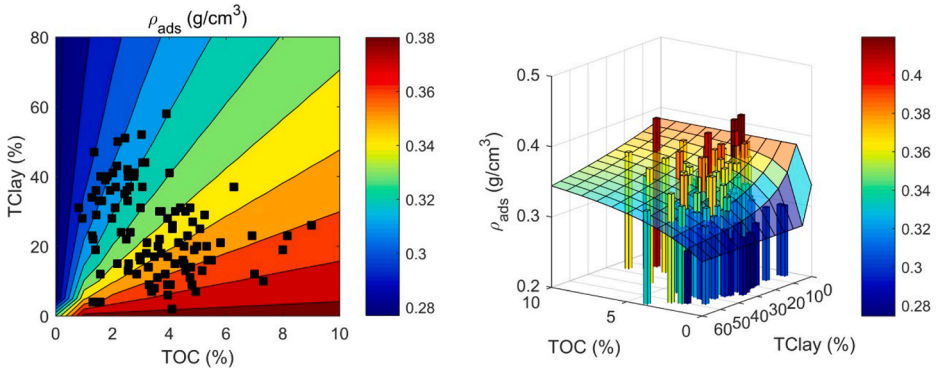

Fig. 17. Variation of ρ_{ads} with TOC and TClay.

composition of shales in other blocks or from different formations might be close to or different from the studied shales here due to the maturity and other factors and further work is needed. However, the framework of this model can be migrated to that might be immature and identify them and inspire the sample selection and make it more targeted, saving cost and time expense.

Declaration of Competing Interest

The authors declare that they have no known competing financial interests or personal relationships that could have appeared to influence the work reported in this paper.

Acknowledgments

This work is supported by the National Natural Science Foundation of China (Grant No. 42030808 and 41690132), the Strategic Priority Research Program of the Chinese Academy of Sciences (Grant No. XDA14010304), the PetroChina Science and Technology Major Project (2019F-31-01), the National Natural Science Foundation of China (41872163).

Appendix A. Supplementary data

Supplementary data to this article can be found online at https://doi.org/10.1016/j.cej.2021.130766.

References

[1] C. Zou, D. Dong, Y. Wang, X. Li, J. Huang, S. Wang, Q. Guan, C. Zhang, H. Wang, H. Liu, W. Bai, F. Liang, W. Lin, Q. Zhao, D. Liu, Z. Yang, P. Liang, S. Sun, Z. Qiu, Shale gas in China: characteristics, challenges and prospects (I), Pet. Explor. Dev. 42 (6) (2015) 753–767, https://doi.org/10.1016/S1876-3804(15)30072-0.

[2] C. Zou, D. Dong, Y. Wang, X. Li, J. Huang, S. Wang, Q. Guan, C. Zhang, H. Wang, H. Liu, W. Bai, F. Liang, W. Lin, Q. Zhao, D. Liu, Z. Yang, P. Liang, S. Sun, Z. Qiu, Shale gas in China: characteristics, challenges and prospects (II), Pet. Explor. Dev. 43 (2) (2016) 182–196, https://doi.org/10.1016/S1876-3804(16)30022-2.

[3] X. Ma, J. Xie, The progress and prospects of shale gas exploration and development in southern Sichuan Basin SW China, Pet. Explor. Dev. 45 (1) (2018) 172–182, https://doi.org/10.1016/S1876-3804(18)30018-1.

[4] X. Ma, J. Xie, R. Yong, Y. Zhu, Geological characteristics and high production control factors of shale gas reservoirs in Silurian Longmaxi Formation, southern Sichuan Basin SW China, Pet. Explor. Dev. 47 (5) (2020) 901–915, https://doi.org/10.1016/S1876-3804(20)60105-7.

[5] Z. Jiang, Y. Song, X. Tang, Z. Li, X. Wang, G. Wang, Z. Xue, X. Li, K. Zhang, J. Chang, H. Qiu, Controlling factors of marine shale gas differential enrichment in southern China, Pet. Explor. Dev. 47 (3) (2020) 661–673, https://doi.org/10.1016/S1876-3804(20)60083-0.

[6] J.M. Ekundayo, R. Rezaee, Numerical simulation of gas production from gas shale reservoirs—influence of gas sorption hysteresis, Energies 12 (2019) 3405, https://doi.org/10.3390/en12183405.

[7] G. Cao, M. Lin, W. Jiang, W. Zhao, L. Ji, C. Li, D. Lei, A statistical-coupled model for organic-rich shale gas transport, J. Petrol. Sci. Eng. 169 (2018) 167–183, https://doi.org/10.1016/j.petrol.2018.05.033.

[8] Z.-Z. Li, T. Min, Q. Kang, Y.-L. He, W.-Q. Tao, Investigation of methane adsorption and its effect on gas transport in shale matrix through microscale and mesoscale simulations, Int. J. Heat Mass Transf. 98 (2016) 675–686, https://doi.org/10.1016/j.ijheatmasstransfer.2016.03.039.

[9] W. Yuan, Z. Pan, X. Li, Y. Yang, C. Zhao, L.D. Connell, S. Li, J. He, Experimental study and modelling of methane adsorption and diffusion in shale, Fuel 117 (2014) 509–519, https://doi.org/10.1016/j.fuel.2013.09.046.

[10] H. Singh, F. Javadpour, Langmuir slip-Langmuir sorption permeability model of shale, Fuel 164 (2016) 28–37, https://doi.org/10.1016/j.fuel.2015.09.073.

[11] P. Chareonsuppanimit, S.A. Mohammad, R.L. Robinson, K.A.M. Gasem, High-pressure adsorption of gases on shales: measurements and modeling, Int. J. Coal Geol. 95 (2012) 34–46, https://doi.org/10.1016/j.coal.2012.02.005.

[12] L. Ji, T. Zhang, K.L. Milliken, J. Qu, X. Zhang, Experimental investigation of main controls to methane adsorption in clay-rich rocks, Appl. Geochem. 27 (12) (2012) 2533–2545, https://doi.org/10.1016/j.apgeochem.2012.08.027.

[13] H. Guo, W. Jia, P. Peng, Y. Lei, X. Luo, M. Cheng, X. Wang, L. Zhang, C. Jiang, The composition and its impact on the methane sorption of lacustrine shales from the Upper Triassic Yanchang Formation Ordos Basin, China, Mar. Pet. Geol. 57 (2014) 509–520, https://doi.org/10.1016/j.marpetgeo.2014.05.010.

[14] M. Gasparik, A. Ghanizadeh, P. Bertier, Y. Gensterblum, S. Bouw, B.M. Krooss, High-pressure methane sorption isotherms of black shales from The Netherlands, Energy Fuels 26 (8) (2012) 4995–5004, https://doi.org/10.1021/ef300405g.

[15] E. Fan, S. Tang, C. Zhang, Q. Guo, C. Sun, Methane sorption capacity of organics and clays in high-over matured shale-gas systems, Energy Explor. Exploit. 32 (6) (2014) 927–942, https://doi.org/10.1260/0144-5987.32.6.927.

[16] M. Gasparik, T.F. Rexer, A.C. Aplin, P. Billemont, G. de Weireld, Y. Gensterblum, M. Henry, B.M. Krooss, S. Liu, X. Ma, R. Sakurovs, Z. Song, G. Staib, K.M. Thomas, S. Wang, T. Zhang, First international inter-laboratory comparison of high-pressure CH 4 CO 2 and C 2 H 6 sorption isotherms on carbonaceous shales, Int. J. Coal Geol. 132 (2014) 131–146, https://doi.org/10.1016/j.coal.2014.07.010.

[17] W. Ji, Y. Song, Z. Jiang, L. Chen, Z. Li, X. Yang, M. Meng, Estimation of marine shale methane adsorption capacity based on experimental investigations of Lower Silurian Longmaxi formation in the Upper Yangtze Platform, south China, Mar. Pet. Geol. 68 (2015) 94–106, https://doi.org/10.1016/j.marpetgeo.2015.08.012.

[18] D. Liu, P. Yuan, H. Liu, T. Li, D. Tan, W. Yuan, H. He, High-pressure adsorption of methane on montmorillonite, kaolinite and illite, Appl. Clay Sci. 85 (2013) 25–30, https://doi.org/10.1016/j.clay.2013.09.009.

[19] T.F. Rexer, E.J. Mathia, A.C. Aplin, K.M. Thomas, High-pressure methane adsorption and characterization of pores in Posidonia Shales and Isolated Kerogens, Energy Fuels 28 (5) (2014) 2886–2901, https://doi.org/10.1021/ef402466m.

[20] T.F.T. Rexer, M.J. Benham, A.C. Aplin, K.M. Thomas, Methane adsorption on shale under simulated geological temperature and pressure conditions, Energy Fuels 27 (6) (2013) 3099–3109, https://doi.org/10.1021/ef400381v.

[21] H.e. Bi, Z. Jiang, J. Li, F. Xiong, P. Li, L. Chen, Ono-Kondo model for supercritical shale gas storage: s case study of Silurian Longmaxi Shale in Southeast Chongqing China, Energy Fuels 31 (3) (2017) 2755–2764, https://doi.org/10.1021/acs.energyfuels.6b03425.

[22] H. Hu, Methane adsorption comparison of different thermal maturity kerogens in shale gas system, Chin. J. Geochem. 33 (4) (2014) 425–430, https://doi.org/10.1007/s11631-014-0708-9.

[23] I. Klewiah, D.S. Berawala, H.C. Alexander Walker, P.Ø. Andersen, P.H. Nadeau, Review of experimental sorption studies of CO2 and CH4 in shales, J. Nat. Gas Sci. Eng. 73 (2020) 103045, https://doi.org/10.1016/j.jngse.2019.103045.

[24] T. Zhang, G.S. Ellis, S.C. Ruppel, K. Milliken, R. Yang, Effect of organic-matter type and thermal maturity on methane adsorption in shale-gas systems, Org Geochem. 47 (2012) 120–131, https://doi.org/10.1016/j.orggeochem.2012.03.012.

[25] L. Chen, L. Zuo, Z. Jiang, S. Jiang, K. Liu, J. Tan, L. Zhang, Mechanisms of shale gas adsorption: evidence from thermodynamics and kinetics study of methane adsorption on shale, Chem. Eng. J. 361 (2019) 559–570, https://doi.org/10.1016/j.cej.2018.11.185.

[26] Z. Feng, F. Hao, S. Zhou, W. Wu, J. Tian, C. Xie, Y. Cai, Pore characteristics and methane adsorption capacity of different lithofacies of the Wufeng Formation-Longmaxi Formation Shales Southern Sichuan Basin, Energy Fuels 34 (7) (2020) 8046–8062, https://doi.org/10.1021/acs.energyfuels.0c00782.

[27] Z. Gao, Y. Fan, Q. Hu, Z. Jiang, Y.u. Cheng, The effects of pore structure on wettability and methane adsorption capability of Longmaxi Formation shale from the southern Sichuan Basin in China, Bulletin 104 104 (6) (2020) 1375–1399, https://doi.org/10.1306/01222019079.

[28] Q. He, T. Dong, S. He, G. Zhai, Methane adsorption capacity of marine-continental transitional facies shales: the case study of the Upper Permian Longtan Formation, northern Guizhou Province, Southwest China, J. Petrol. Sci. Eng. 183 (2019) 106406, https://doi.org/10.1016/j.petrol.2019.106406.

[29] H. Hu, F. Hao, X. Guo, F. Dai, Y. Lu, Y. Ma, Investigation of methane sorption of overmature Wufeng-Longmaxi shale in the Jiaoshiba area Eastern Sichuan Basin, China, Mar. Pet. Geol. 91 (2018) 251–261, https://doi.org/10.1016/j.marpetgeo.2018.01.008.

[30] L. Pan, X. Xiao, H. Tian, Q. Zhou, P. Cheng, Geological models of gas in place of the Longmaxi shale in Southeast Chongqing South China, Mar. Pet. Geol. 73 (2016) 433–444, https://doi.org/10.1016/j.marpetgeo.2016.03.018.

[31] T. Li, H. Tian, X. Xiao, P. Cheng, Q. Zhou, Q. Wei, Geochemical characterization and methane adsorption capacity of overmature organic-rich Lower Cambrian shales in northeast Guizhou region, southwest China, Mar. Pet. Geol. 86 (2017) 858–873, https://doi.org/10.1016/j.marpetgeo.2017.06.043.

[32] R. Hu, W. Wang, J. Tan, L. Chen, J. Dick, G. He, Mechanisms of shale gas adsorption: Insights from a comparative study on a thermodynamic investigation of microfossil-rich shale and non-microfossil shale, Chem. Eng. J. 411 (2021) 128463, https://doi.org/10.1016/j.cej.2021.128463.

[33] F. Xiong, G. Rother, D. Tomasko, W. Pang, J. Moortgat, On the pressure and temperature dependence of adsorption densities and other thermodynamic properties in gas shales, Chem. Eng. J. 395 (2020) 124989, https://doi.org/10.1016/j.cej.2020.124989.

[34] L. Chen, K. Liu, S. Jiang, H. Huang, J. Tan, L. Zuo, Effect of adsorbed phase density on the correction of methane excess adsorption to absolute adsorption in shale, Chem. Eng. J. (2020) 127678, https://doi.org/10.1016/j.cej.2020.127678.

[35] S. Zhou, H. Xue, Y. Ning, W. Guo, Q. Zhang, Experimental study of supercritical methane adsorption in Longmaxi shale: Insights into the density of adsorbed methane, Fuel 211 (2018) 140–148, https://doi.org/10.1016/j.fuel.2017.09.065.

[36] J. Zhang, Y. Tang, D. Chen, Prediction of methane adsorption content in continental coal-bearing shale reservoir using SLD model, Pet. Sci. Technol. 37 (15) (2019) 1839–1845, https://doi.org/10.1080/10916466.2019.1610773.

[37] W. Jiang, M. Lin, Molecular dynamics investigation of conversion methods for excess adsorption amount of shale gas, J. Nat. Gas Sci. Eng. 49 (2018) 241–249, https://doi.org/10.1016/j.jngse.2017.11.006.

[38] Y. Wang, Y. Zhu, S. Liu, R. Zhang, Methane adsorption measurements and modeling for organic-rich marine shale samples, Fuel 172 (2016) 301–309, https://doi.org/10.1016/j.fuel.2015.12.074.

[39] Y. Wang, Y. Zhu, S. Liu, R. Zhang, Pore characterization and its impact on methane adsorption capacity for organic-rich marine shales, Fuel 181 (2016) 227–237, https://doi.org/10.1016/j.fuel.2016.04.082.

[40] C. Zhong, Q. Qin, C. Fan, D. Hu, Effect of nanometer pore structure on methane adsorption capacity in organic-rich shale, Pet. Sci. Technol. 37 (11) (2019) 1243–1250, https://doi.org/10.1080/10916466.2018.1542443.

[41] W. Shi, X. Wang, C. Zhang, A. Feng, Z. Huang, Experimental study on gas content of adsorption and desorption in Fuling shale gas field, J. Petrol. Sci. Eng. 180 (2019) 1069–1076, https://doi.org/10.1016/j.petrol.2019.06.021.

[42] Y. Wang, L. Liu, Y. Sheng, X. Wang, S. Zheng, Z. Luo, Investigation of supercritical methane adsorption of overmature shale in Wufeng-Longmaxi Formation Southern Sichuan Basin, China, Energy Fuels 33 (3) (2019) 2078–2089, https://doi.org/10.1021/acs.energyfuels.8b0434410.1021/acs.energyfuels.8b04344.s001.

[43] R. Yang, S. He, Q. Hu, D. Hu, S. Zhang, J. Yi, Pore characterization and methane sorption capacity of over-mature organic-rich Wufeng and Longmaxi shales in the southeast Sichuan Basin China, Mar. Pe. Geol. 77 (2016) 247–261, https://doi.org/10.1016/j.marpetgeo.2016.06.001.

[44] X. Zhang, W. Shi, Q. Hu, S. Zhang, H. Hu, X. Wang, Z. Xu, Geological controls and methane sorption capacity of marine shales of the Fuling shale gas field in the eastern Sichuan Basin China, Pet. Geosci. 23 (4) (2017) 466–475, https://doi.org/10.1144/petgeo2016-064.

[45] T. Zhao, X. Li, Z. Ning, H. Zhao, J. Zhang, W. Zhao, Pore structure and adsorption behavior of shale gas reservoir with influence of maturity: a case study of Lower Silurian Longmaxi formation in China, Arab J Geosci 11 (13) (2018), https://doi.org/10.1007/s12517-018-3673-5.

[46] F. Yang, C. Xie, S. Xu, Z. Ning, B.M. Krooss, Supercritical methane sorption on organic-rich shales over a wide temperature range, Energy Fuels 31 (12) (2017) 13427–13438, https://doi.org/10.1021/acs.energyfuels.7b02628.

[47] J.M. Ekundayo, R. Rezaee, Effect of equation of states on high-pressure volumetric measurements of methane-coal sorption isotherms—Part 1: Volumes of free space and methane adsorption isotherms, Energy Fuels 33 (2) (2019) 1029–1036, https://doi.org/10.1021/acs.energyfuels.8b0401610.1021/acs.energyfuels.8b04016.s001.

[48] U. Setzmann, W. Wagner, A new equation of state and tables of thermodynamic properties for methane covering the range from the melting line to 625 K at pressures up to 100 MPa, J. Phys. Chem. Ref. Data 20 (6) (1991) 1061–1155, https://doi.org/10.1063/1.555898.

[49] C.M. Jarque, A.K. Bera, A Test for normality of observations and regression residuals, International Statistical Review / Revue Internationale de Statistique 55 (1987) 163. https://doi.org/10.2307/1403192.

[50] R.J. Ambrose, R.C. Hartman, M. Diaz-Campos, I.Y. Akkutlu, C.H. Sondergeld, Shale gas-in-place calculations part I: new pore-scale considerations, SPE J. 17 (2012) 219–229, https://doi.org/10.2118/131772-PA.

[51] J.L. Rodgers, W.A. Nicewander, Thirteen ways to look at the correlation coefficient, The Amer. Statist. 42 (1) (1988) 59, https://doi.org/10.2307/2685263.

[52] D.N. Reshef, Y.A. Reshef, H.K. Finucane, S.R. Grossman, G. McVean, P. J. Turnbaugh, E.S. Lander, M. Mitzenmacher, P.C. Sabeti, Detecting novel associations in large data sets, Science 334 (6062) (2011) 1518–1524, https://doi.org/10.1126/science:1205438.

[53] D. Albanese, M. Filosi, R. Visintainer, S. Riccadonna, G. Jurman, C. Furlanello, Minerva and minepy: a C engine for the MINE suite and its R Python and MATLAB wrappers, Bioinformatics 29 (2013) 407–408, https://doi.org/10.1093/bioinformatics/bts707.

[54] M. Gasparik, P. Bertier, Y. Gensterblum, A. Ghanizadeh, B.M. Krooss, R. Littke, Geological controls on the methane storage capacity in organic-rich shales, Int. J. Coal Geol. 123 (2014) 34–51, https://doi.org/10.1016/j.coal.2013.06.010.

[55] E. Borgonovo, E. Plischke, Sensitivity analysis: a review of recent advances, Eur. J. Oper. Res. 248 (3) (2016) 869–887, https://doi.org/10.1016/j.ejor.2015.06.032.

[56] H. Tian, T. Li, T. Zhang, X. Xiao, Characterization of methane adsorption on overmature Lower Silurian-Upper Ordovician shales in Sichuan Basin, southwest China: experimental results and geological implications, Int. J. Coal Geol. 156 (2016) 36–49, https://doi.org/10.1016/j.coal.2016.01.013.

[57] P. Li, Z. Jiang, M. Zheng, H. Bi, L. Chen, Estimation of shale gas adsorption capacity of the Longmaxi Formation in the Upper Yangtze Platform China, J. Natural Gas Sci. Eng. 34 (2016) 1034–1043, https://doi.org/10.1016/j.jngse.2016.07.052.

[58] J. Wu, Y. Yuan, S. Niu, X. Wei, J. Yang, Multiscale characterization of pore structure and connectivity of Wufeng-Longmaxi shale in Sichuan Basin China, Mar. Pet. Geol. 120 (2020) 104514, https://doi.org/10.1016/j.marpetgeo.2020.104514.

[59] F. Yang, Z. Ning, R. Zhang, H. Zhao, B.M. Krooss, Investigations on the methane sorption capacity of marine shales from Sichuan Basin China, Int. J. Coal Geol. 146 (2015) 104–117, https://doi.org/10.1016/j.coal.2015.05.009.

[60] K. Gao, G.-J. Guo, M. Zhang, Z. Zhang, B.o. Peng, Nanopore surfaces control the shale gas adsorption via roughness and layer-accumulated adsorption potential: a molecular dynamics study, Energy Fuels 35 (6) (2021) 4893–4900, https://doi.org/10.1021/acs.energyfuels.0c04322.

[61] X. Tang, N. Ripepi, N.P. Stadie, L. Yu, M.R. Hall, A dual-site Langmuir equation for accurate estimation of high pressure deep shale gas resources, Fuel 185 (2016) 10–17, https://doi.org/10.1016/j.fuel.2016.07.088.

[62] J. Zou, R. Rezaee, K. Liu, Effect of temperature on methane adsorption in shale gas reservoirs, Energy Fuels 31 (11) (2017) 12081–12092, https://doi.org/10.1021/acs.energyfuels.7b02639.